

## Measurement of Solar Differential Rotation by Absolutely Calibrated Iodine-Cell Spectroscopy

Yoichi Takeda●●

© The author(s) ●●●●

**Abstract** The iodine-cell technique, which is known to be efficient in precisely establishing Doppler velocity shifts, was once applied by the author to measuring the solar differential rotation based on full-disk spectroscopic observations (Takeda and Ueno, *Sol. Phys.* **270**, 447, 2011). However, the data reduction procedure (in simple analogy with the stellar case) adopted therein was not necessarily adequate, because specific characteristic involved with the disk-resolved Sun (i.e., center–limb variation of line strengths) was not properly taken into consideration. Therefore, this problem is revisited based on the same data but with an application to theoretical spectrum fitting, which can yield absolute heliocentric radial velocities ( $v_{\text{obs}}$ ) in a consistent manner as shown in the study of solar gravitational redshift (Takeda and Ueno, *Sol. Phys.* **281**, 551, 2012). Likewise, instead of converting  $v_{\text{obs}}$  into  $\omega$  (angular velocity) at each disk point, which suffers considerable errors especially near the central meridian,  $\omega$  was derived this time by applying the least squares analysis to a dataset comprising  $v_{\text{obs}}$  values at many points. This new analysis resulted in  $\omega$  ( $\text{deg day}^{-1}$ ) =  $13.92(\pm 0.03) - 1.69(\pm 0.34) \sin^2 \psi - 2.37(\pm 0.62) \sin^4 \psi$  ( $\psi$ : the heliographic latitude) along with the gravitational redshift of  $675 \text{ m s}^{-1}$ , which are favorably compared with previous publications. In addition, how the distribution of observing points on the disk affects the result is also examined, which reveals that rotation parameters may suffer appreciable errors depending on cases.

**Keywords:** Center-Limb Observations — Instrumentation and Data Management — Rotation — Spectrum, Visible — Velocity Fields, Photosphere

---

Y. Takeda  
[ytakeda@js2.so-net.ne.jp](mailto:ytakeda@js2.so-net.ne.jp)

11-2 Enomachi, Naka-ku, Hiroshima-shi 730-0851, Japan

arXiv:2406.18271v1 [astro-ph.SR] 26 Jun 2024

## 1. Introduction

### 1.1. Past Studies of Solar Differential Rotation

Ever since Christoph Scheiner noticed about 400 years ago from sunspots observations that the Sun rotates with a shorter period in the equator than in higher latitudes, a number of observational studies on this “solar differential rotation” were conducted especially in the 20th century (mainly by invoking two approaches of sunspot tracing and spectroscopic Doppler method), and various information on its characteristics has been accumulated. Moreover, the advent of solar seismology has enabled to diagnose the nature of internal rotation successfully. See, e.g., Paternò (2010) for a review concisely summarizing the historical aspect and current status on this subject.

Nowadays, observationally studying the surface differential rotation on the visible solar disk is rather classical and not the mainstream of solar physics, given that the main features had been established in 1970s–1980s as reviewed by Schröter (1985). In the author’s opinion, however, it is still important and worth pursuing to improve the precision of the rotational parameters as much as possible, in order to clarify their dependence upon the solar activity cycle since both should be closely connected through the dynamo mechanism.

From the viewpoint of accomplishing higher accuracy, the spectroscopic approach (quickly yielding the result and potentially applicable to any higher latitude) may be superior to the tracing method (which requires a rather long monitoring and is limited up to a certain latitude depending on the activity phase).

Since radial velocities<sup>1</sup> at many points on the solar disk have to be efficiently determined in this case (for which classical manual work on the spectra is hardly practicable), the best choice would be the Doppler compensator method by using a magnetograph (e.g., Howard and Harvey, 1970). Actually, most of the spectroscopic measurements of solar differential rotation over the past half century (mainly in 1960s–1980s) have employed this technique (see, e.g., Schröter, 1985, and the references therein).

But unfortunately, this method is not necessarily easy to practice from the technical as well as budgetary point of view, because it requires an instrument manufactured with skill and carefully tuned. Accordingly, application of this technique to solar differential rotation measurement was experienced mainly in large observatories (e.g., Mt. Wilson or Kitt Peak).

### 1.2. Iodine Cell as an Effective Spectroscopic Tool

Here, the iodine-cell spectroscopy may serve as a promising alternative, because it also enables fairly precise measurement of Doppler shifts based on efficient

---

<sup>1</sup>Following the usual astronomical convention, we use the term “radial velocity” for the velocity component along the line of sight (positive for the direction towards recession) in this article. Note, however, that this terminology is not so widely used in solar physics (for which “line-of-sight velocity” may be more preferred), presumably because the adjective “radial” is rather confusing in distinguishing from the meaning of center-to-limb direction on the solar disk.

data reduction procedures using an optimization algorithm. This method became very popular in application to searching for extrasolar planets around stars, although it was originally introduced in solar physics. The decisive merit of this technique is its simplicity and cost effectiveness: what should be done is only to place the gas filter containing iodine vapor somewhere in the light path of the spectrograph.

A trial of applying the iodine-cell technique to measurement of solar differential rotation was done by Takeda and Ueno (2011; hereinafter referred to as Paper I) based on full-disk spectroscopic observations, which yielded results more or less reasonable. However, some unsatisfactory drawbacks are noticed in the data reduction procedures adopted in that work as described below.

### *1.2.1. Disregarded Center–Limb Spectral Variation*

Firstly, an alarming weakpoint was the choice of the reference spectrum. The essence of data analysis in the iodine-cell method is to simulate the “object+iodine” spectrum (to be compared with the observed one) based on the (i) “pure iodine” spectrum and (ii) “pure object” (reference) spectrum appropriately Doppler-shifted. In Paper I, the solar disk-center spectrum was adopted as the representative reference spectrum throughout the analysis (see Section 3 therein). This assumption means that the center–limb spectral variation, differing from line to line as extensively studied by Takeda and UeNo (2019), was neglected, which must have lead to some imperfect match between the simulated and observed spectra (especially near to the limb). This is presumably the reason for the fact that the resulting radial velocities fluctuated and their errors were appreciably position-dependent.

A remedy for this problem (in order to appropriately handle disk-resolved solar spectra by correctly taking into account the center–limb variation) is to use “theoretical reference spectra” which are so modeled as to well reproduce observed solar spectra by adequately adjusting the parameters (abundances, line broadening, etc.). This approach was soon later adopted by Takeda and Ueno (2012; hereinafter Paper II) in the trial of detecting the solar gravitational redshift, since “absolute” radial velocities are obtained in this case. Although the precision itself attained in such an absolute analysis is quantitatively lower as compared to the case of purely relative analysis (as done in Paper I), it has a merit that errors in the velocity solutions are guaranteed to be consistently uniform, which should be more essential in the present context. Accordingly, it is worth reinvestigating the nature of solar differential rotation based on the model-based analysis as done in Paper II. Since heliocentric radial velocities in the absolute scale are usable in this case, there is no need to make use of the symmetry about the central meridian (which has been adopted in almost all solar rotation studies) and the gravitational redshift can be simultaneously derived as a by-product based on the full-disk data.

### *1.2.2. Inadequate Derivation of Angular Velocity*

Secondly, regarding the evaluation of the rotational angular velocity ( $\omega$ ) as a function of heliographic latitude ( $\psi$ ) based on the observed radial velocities ( $v_{\text{obs}}$ )

at each of the many points  $(x, y)$  on the disk, the procedure adopted in Paper I was not necessarily adequate. That is,  $\omega_i(\psi_i)$  was “directly” derived from  $v_{\text{obs},i}$  at each individual point  $(x_i, y_i)$ , because  $\omega$  is analytically related to  $v_{\text{obs}}$ . The final  $\omega$  versus  $\psi$  relation (parameterized as a second-order polynomial in terms of  $\sin^2 \psi$ ) was determined from the least squares analysis based on the resulting set of  $\omega_i(\psi_i)$  ( $i = 1, 2, \dots, N$ ).

The problematic point is, since  $\omega(\propto v_{\text{obs}}/x)$  is almost inversely proportional to  $x$  (distance from the meridian along the east–west direction), even small errors involved in  $v_{\text{obs}}$  are considerably enhanced when converted to  $\omega$  if  $|x|$  is small. As a matter of fact, those  $\omega_i$  data at  $|x_i| < 0.3R$  ( $R$  is the solar radius) had to be discarded in Paper I, which was a big waste because more than half of the total points could not be used. Besides,  $\omega_i$  data of diversified error sizes had to be combined, which was not sound.

A much better way of analysis should be to determine  $\omega(\psi)$  from the “ensemble” of  $v_{\text{obs}}$  data themselves (instead of directly converting  $v_{\text{obs}}$  to  $\omega$  at each point) by applying the least square analysis, such as previously done by Howard and Harvey (1970). Therefore, we analyze the radial velocity data by following this approach, where two different cases are examined: (a)  $\omega(\psi)$  is expressed by a quadratic polynomial in terms of  $\sin^2 \psi$  and their parameters are determined based on all  $v_{\text{obs}}$  data, and (b)  $\omega$  is determined from the  $v_{\text{obs}}$  data belonging to each  $\psi$  bin of  $10^\circ$  wide (without postulating any analytic expression of  $\omega$  versus  $\psi$  relation). It would be interesting to check where both results satisfactorily agree with each other.

### 1.3. Objectives of This Study

Accordingly, being motivated to overcome the problems involved in Paper I, the purpose of this investigation is (i) to reanalyze the same observational data to yield absolute  $v_{\text{obs}}$  by the model-based procedure employed in Paper II, and (ii) to derive  $\omega$  as a function of  $\psi$  by applying the least squares analysis to the data set of  $v_{\text{obs}}$ .

Also, as a by-product of the present analysis of full-disk radial velocities, the solar gravitational redshift should be obtained. It is interesting to compare this value with that obtained in Paper II, which was obtained only from the meridian data free from rotation.

In addition, as a related application, we study how the distribution of observed points on the disk (adopted for the analysis) affects the results by examining various test cases, which would be meaningful for understanding the critical factor(s) influencing the precision of rotational parameters. This is another aim of this article.

## 2. Observational Data

The observational data used in this study are the same as adopted in Paper I and Paper II. These high-dispersion spectra covering  $5188\text{--}5212\text{ \AA}$  (imprinted with lines of  $\text{I}_2$  molecules) were obtained by two sets of full-disk covering observations

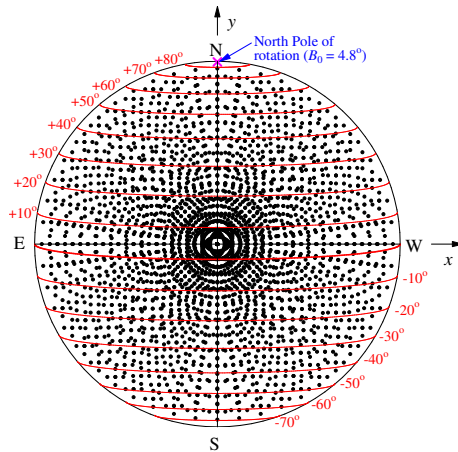


**Figure 1.** Distribution of observed points on the solar disk, at which radial velocities are determined. The loci of constant  $\psi$  (heliographic latitude) are also depicted by red lines.

(on 20–21 July 2010, when the rotational axis is tilted by  $B_0 = +4.8^\circ$ ) done with east–west aligned slits (A-set) and north–south aligned slit (B-set) by using the Domeless Solar Telescope at Hida Observatory of Kyoto University. Each long-slit spectrum was spatially divided into three sub-spectra designated by [l, c, r] (for the A-set) or [t, m, b] (for the B-set). Therefore, two characters (such as “A1” or “Bm”) are assigned to each (sub-)spectrum to discern the corresponding spacial position (relative to the slit center) on the disk. Since the scanning over the disk was done with  $\Delta r = R/12$  (step of radial direction) and  $\Delta\theta = 360^\circ/48$  (step of position angle) for both sets, spectra at 3456 ( $= 2 \times 12 \times 48 \times 3$ ) points<sup>2</sup> covering  $r(= \sqrt{x^2 + y^2}) = 0$  (disk center) to  $r = 0.961R$  (near to the limb,  $R$  is the solar radius) are eventually available for the analysis.<sup>3</sup> The corresponding locations of all these spectra on the disk are illustrated in Figure 1. See also Section 2 of Paper I for more detailed descriptions regarding these data.

### 3. Radial Velocity Determination

The procedures of deriving the absolute heliocentric radial velocities ( $v_{\text{obs}}$ ) from the observed spectra at each point of the solar disk are essentially the same as adopted in Paper II (see Sections 3–5 therein). The only difference is that the center–limb variation of the solar photospheric microturbulence ( $\xi$ ) is taken into account (instead of the constant value of  $\xi = 1 \text{ km s}^{-1}$  assumed in Paper II) in fitting the observed spectra with theoretically modeled ones. That is, according

<sup>2</sup>This is the gross number of the observed points in total. There are cases that they happen to positionally overlap with each other.

<sup>3</sup>The spectra observed at the extreme limb (designated by suffix ‘12’ such as  $r_{12}$  in Paper I) are not used in this investigation (as in Paper II) because of their lower reliability.

to the recent work of Takeda (2022),

$$\xi = 1 + 0.0649(1 - \mu) + 1.427(1 - \mu)^2 \text{ (km s}^{-1}\text{)} \quad (1)$$

is adopted (see Equation 1 therein). Here,  $\mu$  is the direction cosine ( $\mu = \cos \Theta$ :  $\Theta$  is the angle between the line of sight and the surface normal), expressed in terms of  $(x, y)$  coordinates as

$$\mu = \sqrt{1 - (x^2 + y^2)/R^2}. \quad (2)$$

The raw radial velocity ( $V_r^{\text{raw}}$ ) at each point (along with the corresponding mean error  $\epsilon$ ) is determined as the mean of the Doppler shifts (after being corrected for offset errors) calculated for four segments of 6 Å wide (cf. Equations 9–11 in Paper II).

Then, the heliocentric radial velocity ( $V_r^{\text{hel}}$ ) is derived by applying the heliocentric correction ( $\Delta^{\text{hel}}$ ; see Section 4.1 in Paper I) as  $V_r^{\text{raw}} + \Delta^{\text{hel}}$ .

Finally, we subtract the correction for the convective blue shift ( $\langle \delta V \rangle$ , cf. Equation 17 in Paper II) from  $V_r^{\text{hel}}$ , which is expressed by the following relation

$$\langle \delta V \rangle = -278.5 + 79.9(1 - \mu) + 422.3(1 - \mu)^2 \text{ (m s}^{-1}\text{)}, \quad (3)$$

in order to obtain the final absolute radial velocity ( $v_{\text{obs}}$ ). Consequently,  $v_{\text{obs}}$  is derived as

$$v_{\text{obs}} = V_r^{\text{raw}} + \Delta^{\text{hel}} - \langle \delta V \rangle. \quad (4)$$

The resulting values of  $V_r^{\text{raw}}$ ,  $\Delta^{\text{hel}}$ ,  $\langle \delta V \rangle$ , and  $v_{\text{obs}}$  at each of the 3456 observed points on the disk are presented in the supplementary online material (tableE.dat).

The histograms for the distribution of errors ( $\epsilon$ , given by Equation 11 in Paper II) involved with  $v_{\text{obs}}$  at each radius bin are depicted in Figure 2a, which shows that no significant dependence exists upon the position on the disk. Actually, their mean value ( $\langle \epsilon \rangle$ ) obtained by averaging  $\epsilon$  is almost constant at  $\approx 80\text{--}90 \text{ m s}^{-1}$  irrespective of  $r$  (Figure 2b), in contrast to the case of Paper I (see Figure 9b therein) where a systematic increase of  $\langle \epsilon \rangle$  with  $r$  toward the limb was observed. Note also that the  $r$ -independent nature of  $\langle \epsilon \rangle$  shown in Figure 2b is favorably more distinct than that in Figure 7b in Paper II (essentially the similar figure), which is presumably due to the reasonable consideration of center–limb variation for  $\xi$  in the present analysis.

Admittedly, the size of  $\epsilon$  itself in the present case of absolute analysis is several times larger in comparison to the relative analysis adopted in Paper I, because various factors<sup>4</sup> are involved as mentioned in Section 6 of Paper II. However, as long as the present purpose (investigating the global feature of rotational velocity field) is concerned, warranting homogeneous precision of  $v_{\text{obs}}$  over the disk should be more significant.

---

<sup>4</sup>For example, since the wavelengths of spectral line data adopted in this analysis have precisions only to the third decimal in Å, this already can be a source of uncertainty amounting to several tens  $\text{m s}^{-1}$  (0.001 Å corresponds to  $\approx 50\text{--}60 \text{ m s}^{-1}$ ).

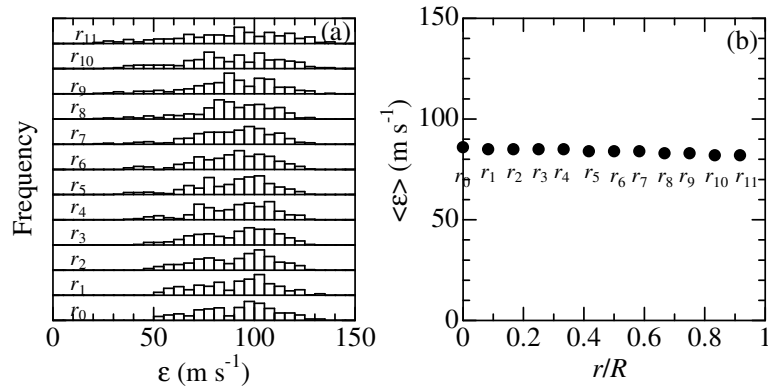


**Figure 2.** (a) Distribution histogram for the errors ( $\epsilon$ ) involved in observed radial velocities at each radius ( $r_0, r_1, \dots, r_{10}, r_{11}$  corresponding to  $r/R = 0, 1/12, \dots, 10/12, 11/12$ ). (b) Averaged errors ( $\langle \epsilon \rangle$ ) calculated at each of the radius bins are plotted against the radius.

#### 4. Trends of Absolute Radial Velocities on the Disk

It is worth examining the global characteristics of the resulting  $v_{\text{obs}}$  in terms of the symmetry with respect to the meridian. In our choice of observed points on the disk, any point in the western hemisphere ( $x^+ (> 0), y$ ) has its symmetric counterpart in the eastern hemisphere ( $x^- (< 0), y$ ), where  $x^+ + x^- = 0$ . Let us denote the radial velocities corresponding to the former and the latter points as  $v_{\text{obs}}^+$  and  $v_{\text{obs}}^-$ , respectively. The four panels of Figure 3 illustrate the correlations of (a)  $v_{\text{obs}}$  versus  $x$ , (b)  $v_{\text{obs}}^+$  versus  $v_{\text{obs}}^-$ , (c)  $0.5(v_{\text{obs}}^+ - v_{\text{obs}}^-)$  versus  $0.5(x^+ - x^-)$ , and (d)  $0.5(v_{\text{obs}}^+ + v_{\text{obs}}^-)$  versus  $y$ . We can see the following trends by inspecting these figures.

- Generally,  $v_{\text{obs}}$  tends to increase with  $x$ , and  $v_{\text{obs}}^+$  and  $v_{\text{obs}}^-$  are inversely correlated with each other.
- The sum of  $0.5(v_{\text{obs}}^+ + v_{\text{obs}}^-)$  is nearly constant, and their average over all pairs is  $0.686 \text{ km s}^{-1}$  (with a standard deviation of  $0.081 \text{ km s}^{-1}$ ).
- This is interpreted as an offset to  $v_{\text{obs}}$  corresponding to the gravitational redshift. If this offset is subtracted,  $v^+ + v^- \approx 0$  is realized, as expected for rotational velocities.
- Accordingly, the global feature of  $v_{\text{obs}}$  is explained mostly by the rotational velocity and an offset constant, which serves as a reference in parameterizing the theoretical radial velocity in Section 5.1.

#### 5. Derivation of the Angular Rotational Velocity

##### 5.1. Case of Assuming an Analytical $\omega$ Versus $\psi$ Relation

As mentioned in Section 4, it is reasonable to include only the rotational velocity component ( $V_{\text{rot}}$ ) plus an offset constant (corresponding to the gravitational

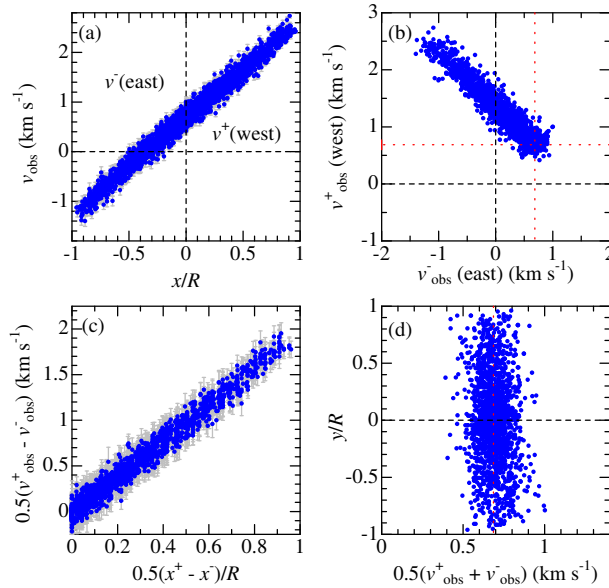


**Figure 3.** Trends of  $v_{\text{obs}}$  (observed absolute radial velocities) in terms of the heliographic coordinates ( $x$  and  $y$ ). Those in the eastern ( $x < 0$ ) and western ( $x > 0$ ) hemispheres are denoted by superscripts “-” and “+”, respectively. (a)  $v_{\text{obs}}$  versus  $x$ . (b)  $v_{\text{obs}}^+$  versus  $v_{\text{obs}}^-$ . (c)  $0.5(v_{\text{obs}}^+ - v_{\text{obs}}^-)$  versus  $0.5(x^+ - x^-)$ , where  $(v_{\text{obs}}^+, v_{\text{obs}}^-)$  and  $(x^+, x^-)$  are the reflectionally symmetric pairs with respect to the meridian. (d)  $0.5(v_{\text{obs}}^+ + v_{\text{obs}}^-)$  versus  $y$ . In panels b and d, the position of  $0.686 \text{ km s}^{-1}$ , which is the average of  $(0.5(v_{\text{obs}}^+ + v_{\text{obs}}^-))$  corresponding to the gravitational redshift, is indicated by the red dotted line. In panels a and c are also shown the error bars in gray.

redshift) in modeling the absolute heliocentric radial velocity to be compared with  $v_{\text{obs}}$ . This implicitly assumes that any locally-fluctuating irregular velocity fields (e.g., supergranules or 5-minutes oscillation) are eventually averaged to become insignificant by using many points on the disk and the global velocity field (e.g., meridional circulation) is quantitatively negligible in comparison with rotation.

The rotational velocity component along the line of sight  $V_{\text{rot}}$  at the heliographic longitude and latitude of  $(\phi, \psi)$ <sup>5</sup> is written as

$$V_{\text{rot}}(\phi, \psi) = R\omega(\psi) \cos \psi \sin \phi \cos B_0, \quad (5)$$

where  $\omega(\psi)$  is the angular velocity at latitude  $\psi$ . The  $(\phi, \psi)$  spherical coordinate system is related to the  $(x, y)$  Cartesian coordinate system on the disk by the following equations.

$$x = R \cos \psi \sin \phi \quad (6)$$

<sup>5</sup>The range of  $\phi$  is  $-180^\circ \leq \phi \leq +180^\circ$ , where  $\phi = 0^\circ$  at the meridian (east/west limb is  $-90^\circ/+90^\circ$ ). The range of  $\psi$  is  $-90^\circ \leq \psi \leq +90^\circ$ , where  $\psi = 0^\circ$  at the equator (south/north pole is  $-90^\circ/+90^\circ$ ).



$$R \sin \psi = \sqrt{R^2 - x^2 - y^2} \sin B_0 + y \cos B_0 \quad (7)$$

Therefore, from Equations 5 and 6,  $V_{\text{rot}}$  is also expressed in the  $(x, y)$  system as

$$V_{\text{rot}}(x, y) = \omega(\psi)x \cos B_0, \quad (8)$$

which indicates that  $V_{\text{rot}}$  is nearly proportional to  $x$  if the weak dependence of  $\omega$  upon the latitude  $\psi$  is disregarded.

As to the latitude dependence of  $\omega$ , we adopt a second-order polynomial in terms of  $\sin^2 \psi$  as usually done,

$$\omega(\psi) = A + B \sin^2 \psi + C \sin^4 \psi, \quad (9)$$

where  $A$ ,  $B$ , and  $C$  are constants.

Therefore, by inserting Equation 9 into Equation 5, the  $\chi^2$  to be minimized by the least squares analysis is expressed as

$$\chi^2 = \sum_{i=1}^N \left[ \frac{v_{\text{obs},i} - x_i \cos B_0 (A + B \sin^2 \psi_i + C \sin^4 \psi_i) - D}{\sigma_i} \right]^2, \quad (10)$$

where  $v_{\text{obs},i}$ ,  $x_i$ ,  $\psi_i$ , and  $\sigma_i (\equiv \epsilon_i)$  correspond to each point  $i$  ( $i = 1, 2, \dots, N$ ), and  $D$  is an offset constant.

The determination of four parameters ( $A$ ,  $B$ ,  $C$ , and  $D$ ) minimizing  $\chi^2$  given by Equation 10 was done by following the standard procedure of least squares analysis (e.g., Bevington and Robinson, 2003), which resulted in<sup>6</sup>  $A = 13.92(\pm 0.03)$ ,  $B = -1.69(\pm 0.34)$ , and  $C = -2.37(\pm 0.62)$  (deg day<sup>-1</sup>), while  $D = 0.675(\pm 0.001)$  (km s<sup>-1</sup>). The corresponding  $\omega$  versus  $\psi$  relation is depicted in Figure 4.

These  $A$ ,  $B$ , and  $C$  values are almost consistent with those derived in Paper I [ $(A, B, C) = (14.03 \pm 0.06, -1.84 \pm 0.57, -1.92 \pm 0.85)$ ] within expected uncertainties, which means that the impact of improvements in this investigation turned out not so remarkable after all. They are also well compared with most results reported in the past publications (see Figure 12 in Paper I), such as that obtained in Mt. Wilson Observatory (Howard and Harvey, 1970) also shown in Figure 4 for comparison.

Regarding the solution of the offset constant  $D$ , its random error in the  $\chi^2$  fitting is considerably small ( $\pm 1$  m s<sup>-1</sup>), reflecting the large number of sample points ( $N = 3456$ ). It should be noted, however, that much larger systematic errors are already involved in the absolute values of the original  $v_{\text{obs}}$  data, especially due to the ambiguity in the adopted formula of the  $\mu$ -dependent convective blue shift given by Equation 3, which are estimated to be on the order of several tens m s<sup>-1</sup> to  $\lesssim 100$  m s<sup>-1</sup> (see Section 6 in Paper II). Accordingly, the  $D$  value of 675 m s<sup>-1</sup> derived from this analysis (similar to the value of 698 m s<sup>-1</sup> obtained in Paper II) is regarded as reasonable in comparison with the true value of the gravitational redshift (633 m s<sup>-1</sup>).

<sup>6</sup>According to the convention,  $A$ ,  $B$ , and  $C$  are expressed in unit of deg day<sup>-1</sup>, which are obtained by multiplying the values in unit of s<sup>-1</sup> ( $=$  km s<sup>-1</sup>/km; since  $v_{\text{obs}}$  and  $x$  are in units of km s<sup>-1</sup> and km, respectively) by  $(180/\pi) \times 24 \times 60 \times 60$ .

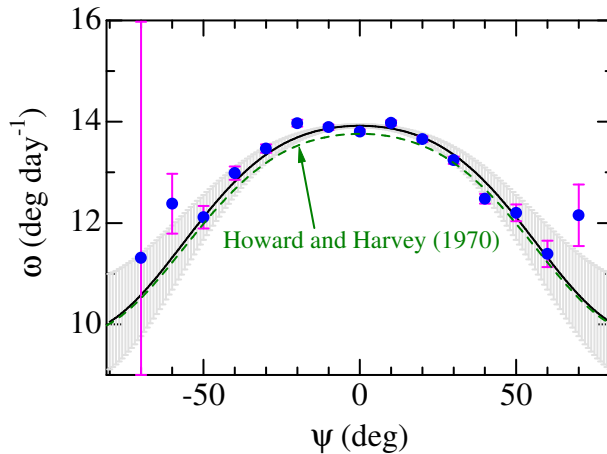


**Figure 4.** The finally obtained  $\omega$  versus  $\psi$  relation,  $\omega = 13.92(\pm 0.03) - 1.69(\pm 0.34) \sin^2 \psi - 2.37(\pm 0.62) \sin^4 \psi$ , is shown by the solid line, where the uncertainty range (corresponding to the errors in  $A$ ,  $B$ , and  $C$ ) is indicated by the gray band. The alternative  $\omega$  solutions derived for 15  $\psi$  bins of  $10^\circ$  wide (cf. Table 1) are also overplotted by blue filled circles (along with error bars). In addition, the  $\omega(\psi)$  curve based on Mt. Wilson observations by Howard and Harvey (1970) is depicted by the dashed line for comparison.

## 5.2. Case of Dividing $\psi$ Into Narrow Bins

Since we may set  $v_{\text{obs}} = V_{\text{rot}} (+ \text{const.})$ , the relation  $v_{\text{obs}}/\cos B_0 = \omega(\psi)x (+\text{const.})$  holds according to Equation 8. Let us consider the case where sample points are in a narrow range of  $\psi$  and thus their  $\omega$ 's are similar to each other. Then,  $v_{\text{obs}}/\cos B_0$  may be regarded as linearly dependent upon  $x$  and its slope (proportionality constant) gives  $\omega$  for this group of data.

Following this idea, all data points are divided according to the values of  $\psi$  into fifteen  $10^\circ$ -bins (centered at  $-70^\circ, -60^\circ, \dots, 0^\circ, \dots, +60^\circ, \text{ and } +70^\circ$ ). Expressing  $v_{\text{obs}}/\cos B_0$  by a linear function  $p + qx$ ,

$$\chi^2 = \sum_{i=1}^N \left[ \frac{v_{\text{obs},i}/\cos B_0 - (p + qx_i)}{\sigma_i} \right]^2 \quad (11)$$

was computed for each bin, where  $\sigma_i \equiv \epsilon_i/\cos B_0$ ,  $p$  is a constant reflecting the gravitational redshift ( $D/\cos B_0$ ), and  $q$  is equivalent to  $\omega$ . The parameters  $p$  and  $q$  were determined by minimizing  $\chi^2$  as done in Section 5.1. The results derived for each of the 15  $\psi$  bins are summarized in Table 1. The  $v_{\text{obs}}$  versus  $x$  plots for each group are illustrated in Figure 4, where the linear-regression lines corresponding to the solutions of  $p$  and  $q$  are also drawn.

The resulting  $\omega$  values are plotted against  $\psi$  in Figure 5 (symbols), in order to compare with the  $\omega(\psi)$  curve determined in Section 5.1 (solid line). We can recognize from this figure that both are in satisfactory agreement at low-to-middle latitude ( $-50^\circ \lesssim \psi \lesssim +50^\circ$ ). However, appreciable discrepancies are seen at higher latitude of  $|\psi| \approx 60-70^\circ$  where the number of available points is

**Table 1.** Results of angular velocity analysis at each latitude bin.

$\psi_m$ (deg)	$[\psi_l, \psi_u]$ (deg)	$N$	$p$ (km s <sup>-1</sup> )	$q \times R^\dagger$ (km s <sup>-1</sup> )	$\omega$ (deg day <sup>-1</sup> )
-70	[-75, -65]	3	0.633(±0.064)	1.589(±0.655)	11.312(±4.662)
-60	[-65, -55]	30	0.700(±0.015)	1.739(±0.083)	12.381(±0.589)
-50	[-55, -45]	70	0.723(±0.010)	1.702(±0.031)	12.113(±0.222)
-40	[-45, -35]	120	0.714(±0.007)	1.824(±0.018)	12.985(±0.132)
-30	[-35, -25]	174	0.708(±0.006)	1.893(±0.012)	13.470(±0.084)
-20	[-25, -15]	264	0.698(±0.005)	1.963(±0.010)	13.970(±0.068)
-10	[-15, -5]	366	0.682(±0.004)	1.952(±0.008)	13.892(±0.055)
+0	[-5, +5]	851	0.666(±0.003)	1.939(±0.006)	13.803(±0.046)
+10	[+5, +15]	607	0.681(±0.003)	1.964(±0.007)	13.976(±0.052)
+20	[+15, +25]	358	0.669(±0.004)	1.919(±0.008)	13.656(±0.056)
+30	[+25, +35]	256	0.660(±0.005)	1.860(±0.010)	13.240(±0.072)
+40	[+35, +45]	170	0.671(±0.006)	1.753(±0.013)	12.479(±0.095)
+50	[+45, +55]	102	0.662(±0.008)	1.714(±0.023)	12.200(±0.165)
+60	[+55, +65]	54	0.669(±0.011)	1.600(±0.037)	11.390(±0.261)
+70	[+65, +75]	28	0.691(±0.014)	1.707(±0.085)	12.152(±0.607)

Note.

$\psi_m$ ,  $\psi_l$ , and  $\psi_u$  are the middle value, lower boundary, and upper boundary of each  $\psi$  bin.  $N$  is the number of data included in each bin.  $p$  and  $q$  are the results of least-square analysis, and  $\omega$  (deg day<sup>-1</sup>) is derived as  $q$  (s<sup>-1</sup>)  $\times$  (180/ $\pi$ )  $\times$  24  $\times$  60  $\times$  60.

<sup>†</sup> $R$ (= 6.955  $\times$  10<sup>5</sup>) is the solar radius in km.

small, which implies that using sufficiently numerous data points is an important factor for precisely determining  $\omega$  by this method.

## 6. Testing Various Distributions of Observing Points

Now that we have obtained the rotational parameters based on all 3456 points covering the solar disk (which are regarded as the “standard solutions”), it may be meaningful to examine how the results are affected in cases of different distributions (where data points are reduced in various ways), by which information of the critical factor(s) may be obtained.

For this purpose, we try three types of test distributions as illustrated in Figure 6, and the results to be compared with the standard “all data” case are presented in Table 2 and Figure 7. Each of the experiments are described below.

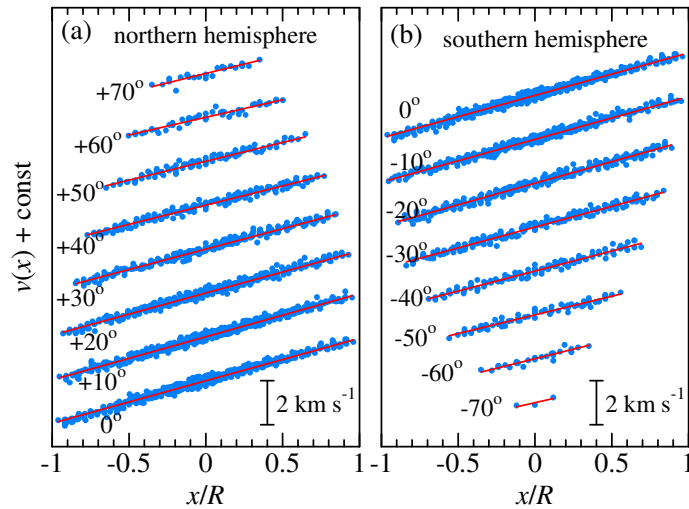


**Figure 5.** The observed  $v_{\text{obs}}$  values belonging to each of the 15  $\psi$ -bins (cf. Table 1) are plotted against  $x$ , where the corresponding linear regression lines (see Table 1 for the best-fit values of  $p$  and  $q$  determined by the least-squares analysis) are also overplotted. The results for each  $\psi$ -bin are vertically shifted by  $2 \text{ km s}^{-1}$  relative to the adjacent ones. (a) Northern hemisphere ( $\psi$  from  $0^\circ$  to  $+70^\circ$ ). (b) Southern hemisphere ( $\psi$  from  $0^\circ$  to  $-70^\circ$ ).

### 6.1. Case (a): Full Disk But with Reduced Density

This test is to examine the impact of reducing the number of points while retaining the fill-disk covering feature. For this purpose, out of the 6 types of sub-spectra (Al, Ac, Ar, Bt, Bm, Bb; see Section 2), (1) only A-set (Al, Ac, Ar), (2) only B-set (Bt, Bm, Bb), and (3) only Ac and Bm, were selected, each of which are called a-1, a-2, and a-3, respectively.

It is interesting to observe from Figure 7a that, while the result for a-1 is reasonably consistent (in the overall sense) with that of all data, those for a-2 and a-3 show appreciable differences despite that their distributions also cover the entire disk (cf. Figure 6). Therefore, although higher density of observing points should generally be more preferable, it is necessary that the points are densely distributed in the E–W direction (like a-1) but not necessarily in the N–S direction (like a-2).

### 6.2. Case (b): Rejecting Points of Near-Meridian Area

This is the test example where any points whose  $|x|$  values (distance from the meridian) within a certain threshold are excluded, which corresponds to the treatment done in Paper I in deriving the final  $\omega$  versus  $\psi$  relation (because of the severely enhanced  $\omega$  errors at small  $|x|$ , cf. Section 1.2.2). Three cases of  $|x|/R > 0.2$  (b-1),  $|x|/R > 0.3$  (b-2, same as in Paper I), and  $|x|/R > 0.4$  (b-3) were tried.

As shown in Figure 7b, the differences from the standard “all data” result turned out insignificant in all of these three cases (b-1, b-2, b-3). This presumably

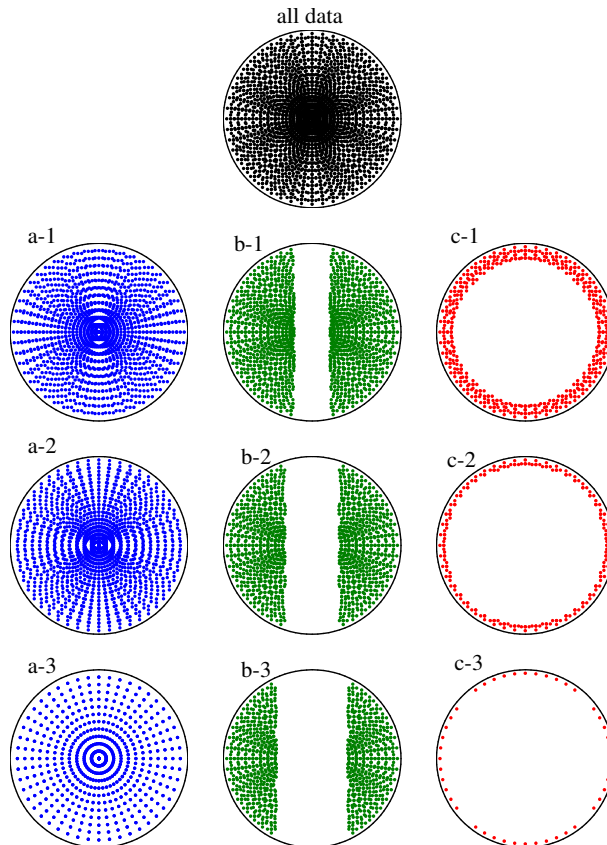


**Figure 6.** Illustrated are the distributions of the data points on the disk, which were adopted for each of the nine test cases described in Table 2. The standard “all data” case is also shown at the top for comparison.

suggests that the behaviors of  $\omega$  are primarily determined by the off-meridian region of larger  $|x|$  where the contribution of  $\omega$  to  $v_{\text{obs}} (\approx \omega x)$  is more significant. Therefore, we may state that the choice of excluding  $|x| < 0.3R$  in Paper I was reasonable (though not well recognized at that time), which may explain the consistency between the results in Paper I and this study (cf. Section 5.1).

### 6.3. Case (c): Only Circular Region Along the Limb

This test is to simulate the case where the observed points are distributed only in the narrow circular band around the limb. As a matter of fact, quite a few spectroscopic determinations of solar rotation (in particular, old ones) relied upon the spectra only near to the limb because the Doppler shift is the largest and easier to detect there. Here, three cases of  $r/R > 0.8$  (c-1),  $r/R > 0.9$  (c-2), and  $r/R > 0.95$  (c-3) are examined.

Figure 7c elucidates that the  $\omega(\psi)$  results for these cases do not match well that of the standard case (especially at higher  $\psi$ ). Although c-1 may still be

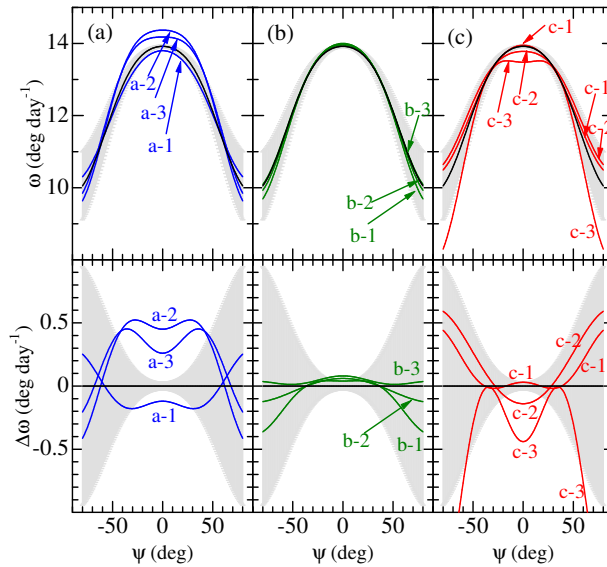


**Figure 7.** Graphical display for the results of nine test calculations (with variously reduced points on the disk, cf. Table 2). (a) Cases of a-1, a-2, and a-3 (in blue). (b) Cases of b-1, b-2, and b-3 (in green). (c) Cases of c-1, c-2, and c-3 (in red). The result for the standard “all data” case is also shown by the black line (with the uncertainty region depicted as the gray band as in Figure 4) for comparison. In each of (a), (b), and (c), the upper panel shows the  $\omega$  versus  $\psi$  relations, while the differences from the “all data” case ( $\Delta\omega$ ) are plotted against  $\psi$  in the lower panel.

regarded as in favorable agreement at lower  $\psi$  (though not good at higher  $\psi$ ), the situation becomes worse at c-2 and c-3 (especially c-3, the most outer distribution, shows a considerable discrepancy). This is presumably related to the fact these Case (c) tests (in particular c-3) are based on much smaller number of points ( $N$ ) compared to Cases (a) and (b) (see Table 2).

## 7. Difficulty of Spectroscopic Solar Rotation Measurement

The test simulations done in Section 6 have shown that spectroscopically determined solar rotation parameters (not only the  $\psi$ -dependent nature of differential rotation but also the equatorial rotation velocity at  $\psi = 0^\circ$ ) depend rather significantly upon how the observed points on the disk are chosen.

Presumably, this is attributed to the irregularly fluctuating velocity components in the solar photosphere. If the velocity field on the solar disk were steady and monotonic, reliable measurement of the rotation law would be feasible based on not so many observing points. However, the actual surface of the Sun is violently in motion and covered with inhomogeneous velocity fields as demonstrated in Figure 8, where the 3D representations of (a)  $v_{\text{obs}}(x, y)$  and (b)  $\Delta v(x, y)$  (residual of  $v_{\text{obs}}$  after subtracting the rotational velocity field  $V_{\text{rot}}$ ) are depicted based on our data. As seen from Figure 8b,  $\Delta v$  shows a random variation on the order of  $\approx 10^2 \text{ m s}^{-1}$ . Therefore, if the distribution of observing

**Table 2.** Tests of how the results are affected by variously reducing the observed points on the disk.

	$N$	$A$	$B$	$C$	$D$	Remark
all data	3456	13.92( $\pm 0.03$ )	-1.69( $\pm 0.34$ )	-2.37( $\pm 0.62$ )	0.675( $\pm 0.001$ )	(Al, Ac, Ar, Bt, Bm, Bb)
(Data of specific slit positions are excluded)						
a-1	1728	13.80( $\pm 0.04$ )	-2.14( $\pm 0.39$ )	-1.51( $\pm 0.72$ )	0.671( $\pm 0.002$ )	only (Al, Ac, Ar)
a-2	1728	14.37( $\pm 0.06$ )	-1.00( $\pm 0.66$ )	-4.00( $\pm 1.18$ )	0.692( $\pm 0.002$ )	only (Bt, Bm, Bb)
a-3	1152	14.18( $\pm 0.06$ )	-0.56( $\pm 0.68$ )	-4.03( $\pm 1.21$ )	0.707( $\pm 0.002$ )	only (Ac, Bm)
(Data within a given distance from the meridian ( $ x $ ) are excluded)						
b-1	1886	13.96( $\pm 0.03$ )	-1.63( $\pm 0.35$ )	-2.86( $\pm 0.65$ )	0.669( $\pm 0.002$ )	only $ x /R > 0.2$
b-2	1430	13.98( $\pm 0.03$ )	-1.85( $\pm 0.37$ )	-2.40( $\pm 0.70$ )	0.666( $\pm 0.002$ )	only $ x /R > 0.3$
b-3	1082	14.00( $\pm 0.03$ )	-1.91( $\pm 0.41$ )	-2.19( $\pm 0.85$ )	0.662( $\pm 0.002$ )	only $ x /R > 0.4$
(Data within a given distance from the disk center ( $r$ ) are excluded)						
c-1	532	13.95( $\pm 0.05$ )	-2.10( $\pm 0.44$ )	-1.51( $\pm 0.74$ )	0.665( $\pm 0.003$ )	only $r/R > 0.8$
c-2	220	13.78( $\pm 0.07$ )	-1.10( $\pm 0.59$ )	-2.20( $\pm 0.93$ )	0.668( $\pm 0.005$ )	only $r/R > 0.9$
c-3	44	13.48( $\pm 0.11$ )	1.00( $\pm 0.87$ )	-6.54( $\pm 1.69$ )	0.649( $\pm 0.012$ )	only $r/R > 0.95$

Note.

$N$  is the total number of adopted data points (see also footnote 2).  $A$ ,  $B$ , and  $C$  are in unit of deg day<sup>-1</sup>, while  $D$  is in km s<sup>-1</sup>. See Figure 6 for the graphical display of the distributions for each of these ten cases.

points is not so dense as to sufficiently cancel out this inhomogeneous velocity fields, incorrect rotation parameters may result.

Accordingly, it is likely that some previously published solar rotation results obtained by Doppler shift measurements (especially those based on comparatively smaller number of observing points) suffered appreciable uncertainties.

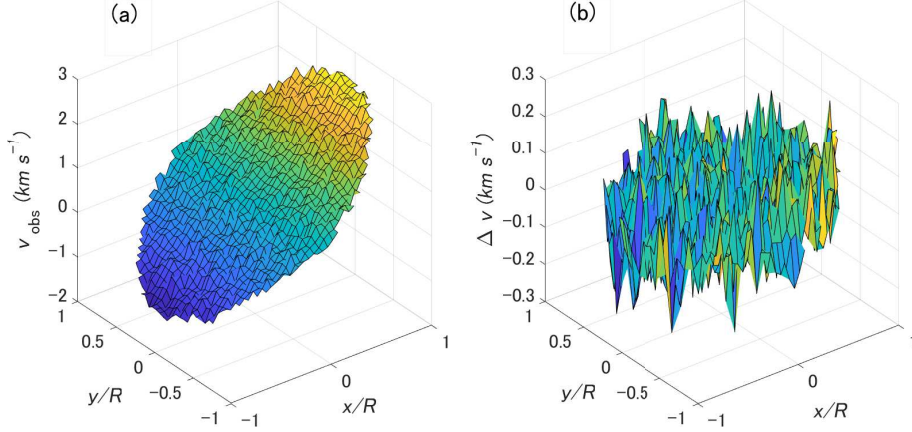


**Figure 8.** 3D representation of (a)  $v_{\text{obs}}(x, y)$  and (b)  $\Delta v(x, y)$ , where the  $x$ - $y$  plane is divided into  $40 \times 40$  square segments. Here,  $\Delta v$  is the difference between  $v_{\text{obs}}$  and  $V_{\text{rot}}$  (rotational velocity field corresponding to the final solutions of  $A$ ,  $B$ ,  $C$ , and  $D$ ).

This may be the cause for the large spread in  $\omega$  versus  $\psi$  curves or some apparent outlier values of  $A$ ,  $B$ ,  $C$  seen in the past historical publications (see, e.g., Figure 2 in Paternò, 2010, or Figure 12 in Paper I). For the same reason, the suspected cyclic variation of solar equatorial rotation velocity (by  $\approx \pm 5\%$ ) with a period of 34 years, which was reported by Belvedere and Paternò (1975) based on the historical publications from 1900 to 1970, had better be viewed with caution.

Nevertheless, the spectroscopic rotational parameters in the “approximate” sense are regarded as being almost established at  $A \approx 14$ ,  $B \approx -2$ , and  $C \approx -2$  based on the literature results (see Figure 12 in Paper I). Yet, what is required for proceeding to the next step (e.g., to detect the dependence of rotation upon the activity phase as mentioned in Section 1) should be to further improve the precision of determination. Though this is not an easy task for which nobody knows any definite recipe, what should be generally kept in mind may be summarized into the following two points.

- First, it is essentially important to employ spectra obtained at as many (i.e., densely distributed) observing points as possible. Regarding their distribution, more weight (higher density) should be given to larger  $x$  region as well as to E–W direction according to the results in Section 6.
- Second, even if using many points on the disk could be accomplished, only one set of data acquired in a short time (e.g., in  $\approx 1$  day) is not sufficient to warrant the reliability of the solution. Comparing the results derived by analyzing several or more sets of data based on repeated observations over a certain period would help to estimate the real precision quantitatively.

## 8. Summary and Conclusion

In studying the solar differential rotation on the visible surface, two representative methods have been traditionally employed: (i) tracing of active regions (such as sunspots) over the rotation cycle and (ii) spectroscopic Doppler shift measurement on the disk.

Following the latter spectroscopic approach, Takeda and Ueno once investigated in Paper I the nature of solar differential rotation based on the full-disk observations by applying the  $I_2$ -cell technique, which is known to be efficient in precise determinations of Doppler velocity shifts.

As viewed from the present knowledge, however, the procedure of analyzing  $I_2$ +solar composite spectrum adopted in that paper was problematic in the sense that the center–limb variation of spectral line strengths was not taken into consideration, because the disk-center spectrum was exclusively used as the reference spectrum. In addition, the derivation of  $\omega$  done in Paper I was not necessarily adequate because it was directly converted from  $v_{\text{obs}}$  at each point of the disk, which eventually resulted in considerable errors in  $\omega$  at smaller  $x$  near to the meridian.

The remedy for the former problem is to use an adequately adjusted theoretical spectrum as the comparison reference at each point as done in Paper II (where the gravitational redshift was determined from the meridian data), by which



absolute heliocentric radial velocity can be obtained. Meanwhile, the solution for the latter problem is to derive  $\omega$  (not one-by-one from each  $v_{\text{obs}}$  but) from an “ensemble” of  $v_{\text{obs}}$  data by applying the least squares analysis.

Motivated by these considerations, the author decided to redetermine the parameters of solar differential rotation based on absolute radial velocities, which were derived from the same observational data as used in Paper I but by applying the analysis procedure devised in Paper II.

In deriving the  $\omega$  versus  $\psi$  relation, two different approaches were tried. (a) Expressing  $\omega$  by 2nd-order polynomial in terms of  $\sin^2 \psi$ , a least-squares analysis was applied to the whole  $v_{\text{obs}}$  data over the disk to derive  $A$ ,  $B$ , and  $C$  (coefficients of the polynomial) and  $D$  (gravitational redshift). (b) All data points were divided according to  $\psi$  into fifteen  $10^\circ$ -bins, and a linear regression analysis was applied to  $v_{\text{obs}}$  data belonging to each  $\psi$ -bin to determine the corresponding  $\omega$ .

The first approach resulted in  $\omega$  ( $\text{deg day}^{-1}$ ) =  $13.92(\pm 0.03) - 1.69(\pm 0.34) \sin^2 \psi - 2.37(\pm 0.62) \sin^4 \psi$  along with the gravitational redshift of  $675 \text{ m s}^{-1}$ . Meanwhile, the  $\omega$  values derived by the second approach at each of the  $\psi$ -bins are in good agreement at low-to-middle latitude ( $-50^\circ \lesssim \psi \lesssim +50^\circ$ ), though appreciable discrepancies are seen at higher latitude ( $|\psi| \approx 60-70^\circ$ ) where the number of available points is small.

This  $\omega$  versus  $\psi$  relation is almost consistent with that obtained in Paper I, which means that the changes in the results are insignificant despite of the updated procedures in this new analysis. Likewise, these  $A$ ,  $B$ ,  $C$  values are favorably compared with those of previous publications (see Figure 12 in Paper I).

As a related application of this analysis, the impact of reducing the number of observing points was also examined. This test revealed that significant changes of rotation parameters are observed in some cases, which is presumably due to the irregular velocity field on the solar surface. It is necessary, therefore, to pay attention to secure a sufficiently large number of points on the disk, in order to obtain reliable results of higher precision.

**Acknowledgements** This investigation has made use of the data obtained by using the Domeless Solar Telescope at Hida Observatory of Kyoto University.

**Data Availability** The radial velocity data and related quantities at each point of the solar disk, upon which this study is based, are available as supplementary material online (ReadMe.txt, tableE.dat).

## Declarations

**Conflict of interest** The author declares that he has no conflicts of interest.

## References

- Belvedere, G., Paternò, L.:1975, *Sol. Phys.* **41**, 289. DOI: 10.1007/BF00154066  
Bevington, P.R., Robinson, D.K.: 2003, *Data Reduction and Error Analysis for the Physical Sciences*, 3rd ed., McGraw Hill, New York.  
Howard, R., Harvey, J.: 1970, *Sol. Phys.* **12**, 23. DOI: 10.1007/BF02276562

- Paternò, L.: 2010, *Astrophys. Space Sci.* **328**, 269. DOI: 10.1007/s10509-009-0218-0
- Schröter, E.H.: 1985, *Sol. Phys.* **100**, 141. DOI: 10.1007/BF00158426
- Takeda, Y.: 2022, *Sol. Phys.* **297**, 4. DOI: 10.1007/s11207-021-01931-0
- Takeda, Y., Ueno, S.: 2011, *Sol. Phys.* **270**, 447 (Paper I). DOI: 10.1007/s11207-011-9765-y
- Takeda, Y., Ueno, S.: 2012, *Sol. Phys.* **281**, 551 (Paper II). DOI: 10.1007/s11207-012-0068-8
- Takeda, Y., UeNo, S.: 2019, *Sol. Phys.* **294**, 63. DOI: 10.1007/s11207-019-1455-1